· Article ·
doi: 10.13679/j.advps.2015.2.00168

Advances in Polar Science
June 2015 Vol. 26 No. 2: 168-178

Model simulations of the annual cycle of the landfast ice thickness in the East Siberian Sea

YANG Yu[1*], Matti Leppäranta[2], LI Zhijun[3], Bin Cheng[4], ZHAI Mengxi[2,5] & Denis Demchev[6]

[1] Department of Basic Sciences, Shenyang Institute of Engineering, Shenyang 110136, China;
[2] Department of Physics, University of Helsinki, Fi-00014 Helsinki, Finland;
[3] State Key Laboratory of Coastal and Offshore Engineering, Dalian University of Technology, Dalian 116024, China;
[4] Finnish Meteorological Institute, Fi-00101 Helsinki, Finland;
[5] Beijing Normal University, Beijing100875, China;
[6] Nansen International Environmental Remote Sensing Centre (NIERSC), Saint-Petersburg 199034, Russia

Received 14 November 2014 ; accepted 7 May 2015

Abstract The annual cycle of the thickness and temperature of landfast sea ice in the East Siberian Sea has been examined using a one-dimensional thermodynamic model. The model was calibrated for the year August 2012–July 2013, forced using the data of the Russian weather station Kotel'ny Island and ECMWF reanalyses. Thermal growth and decay of ice were reproduced well, and the maximum annual ice thickness and breakup day became 1.64 m and the end of July. Oceanic heat flux was 2 $W \cdot m^{-2}$ in winter and raised to 25 $W \cdot m^{-2}$ in summer, albedo was 0.3–0.8 depending on the surface type (snow/ice and wet/dry). The model outcome showed sensitivity to the albedo, air temperature and oceanic heat flux. The modelled snow cover was less than 10 cm having a small influence on the ice thickness. *In situ* sea ice thickness in the East Siberian Sea is rarely available in publications. This study provides a method for quantitative ice thickness estimation by modelling. The result can be used as a proxy to understand the sea ice conditions on the Eurasian Arctic coast, which is important for shipping and high-resolution Arctic climate modelling.

Keywords **landfast sea ice, New Siberian Islands, ice growth, ice decay, oceanic heat flux, snow, albedo**

Citation: Yang Y, Leppäranta M, Li Z J, et al. Model simulations of the annual cycle of the landfast ice thickness in the East Siberian Sea. Adv Polar Sci, 2015, 26: 168-178, doi: 10.13679/j.advps.2015.2.00168

1 Introduction

In Arctic seas, the thermodynamic growth of first-year sea ice is at most about 2 m[1]. Different growth mechanisms produce layers of different ice classes. In the Arctic coast congelation ice is strongly dominant, while frazil ice and platelet ice may be observed at river mouths to a minor degree[2]. Growth of ice is forced by heat losses to the atmosphere, which take out the latent heat released in the formation of ice crystals, while solar, atmospheric and oceanic heat gains cause sea ice melting. Solar radiation is able to penetrate the ice surface and cause internal melting of the ice cover. Sea ice is a thin film in that its capacity to store heat is low, and volume changes consequently follow external forcing with a small time lag. When surviving over summer, sea ice becomes multi-year ice and may reach thicknesses of 3–5 m by thermal growth in the course of several years[3-4].

In the recent 30 years, the Arctic sea ice has rapidly become thinner. In the period 1980–2008 the winter ice thickness in the central Arctic decreased by approximately 1.8 m[5], which is strongly related to the reduction of the area

* Corresponding author (email: yangyang-0606@hotmail.com)

covered by multiyear ice. In the Russian Arctic as well, sea ice concentration and thickness revealed remarkable changes. In particular, satellite data analyses have shown a large reduction in the summer sea ice extent in all Russian Arctic seas. In September 2008, the record minimum ice extent was observed in the East Siberian Sea[6].

Sea ice thickness in the Eurasian Arctic Ocean has been investigated in early 1990s. The average thickness of multi-year level ice was 2.86 m in August[7]. This is significantly less than earlier results[4,8]. The first documented landfast ice thickness chart in the Eurasian continental shelf (Figure 1) was based on observations and results from a calibrated analytical ice thickness model applied for ice season 1938/1939[3]. The maximum annual landfast ice thickness was about 1.8 m in the East Siberian Sea decreasing from there toward west to 1.2–1.5 m in the Kara Sea and toward east to 1.5 m in the Chukchi Sea. The variations of landfast ice thickness are primarily dictated by air temperature and snow accumulation. Along the Taymyr Peninsula, the landfast ice may survive over the summer season to become multi-year ice[9].

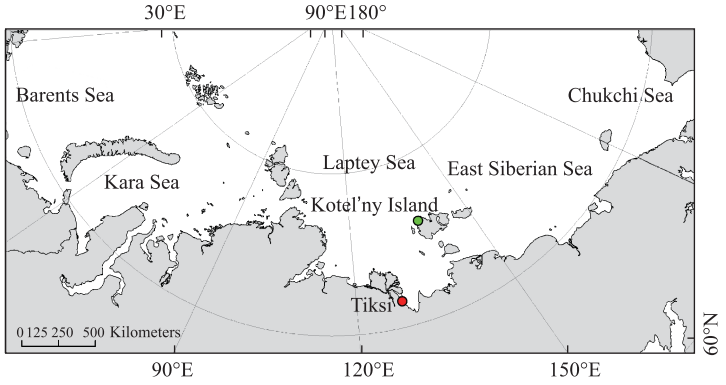

Figure 1 The Arctic Ocean along the Russian coast. The study site (green dot) was in the west coast of the Kotel'ny Island. Tiksi is marked with a red dot.

The rapid Arctic sea ice retreat in recent years has affected also landfast ice thickness in the East Siberian and Laptev seas. Long-term measurements have indicated a steady decreasing trend in May[10]. The upper limit of ice thickness is observed in the East Siberian Shelf[11], while toward the west the thickness is less. The reason is the warmer climate in Northeast Europe. In summer, the air temperature is close to 0℃ in the coastal zone, and the melting process is accelerated by the albedo feedback mechanism. Oceanic heat flux is the least known external forcing factor in sea ice thermodynamics in the region. In the Central Arctic Ocean, 2 $W \cdot m^{-2}$ is widely considered as a reasonable annual average value[12-13], but in the Siberian coast it may be larger in summer due to river inflow and the presence of wide open water zones. The influence of snow cover and turbulent heat fluxes are also important factors.

Congelation ice is the dominant ice type in the Eurasian landfast ice[9-10]. In the annual first-year sea ice cycle, ice disappears in late summer (August–September) due to melting and transport, and then after summer new ice begins to grow in the open water. Likewise, in Siberian lakes all ice melts in summer. The Eurasian landfast ice zone is wide due to the shallow continental shelf[9]. The landfast ice zone extends to the depths of 20 m, up to 200 km from the shoreline at the New Siberian Islands[3].

Sea ice modelling work in Arctic seas has mainly consisted of two-dimensional dynamic-thermodynamic models for large basins with no particular attention to the mechanics of landfast ice[14]. One-dimensional, pure thermodynamic sea ice models have been employed for investigations of thermal growth and decay of ice. Although the large-scale models deliver reasonable general features of the spatial distribution of sea ice thickness, they do not provide the detail temperature distribution, layer structure, ice thickness cycle, and as well the sea ice properties, which depend on the temperature and stratigraphy.

Sea ice thermodynamic modelling is performed along two lines. First, analytic or semi-analytic models of ice growth ignore thermal inertia and penetration of solar radiation into the ice[1,15]. In that case, the temperature profile is piecewise linear. These models can be called quasi-steady models, since the temperature profile immediately shifts into a new steady-state form when the boundary conditions change. During the process of ice melt there is no conduction but the external fluxes melt the ice at the boundaries and by the solar radiation and brine dynamics also in the interior. Melting can therefore be predicted as soon as the total heat flux into the ice is given.

Secondly, time-dependent models are based on a direct numerical solution of the thermal conduction equation. They may have coarse resolution[16-17] or high resolution with 0.05–0.10 m grid size[4,18-23]. High-resolution models are well capable of resolving the response of ice to daily cycles in external forcing. The thermal diffusion coefficient of sea ice is ~0.1 $m^2 \cdot d^{-1}$ and therefore the length scale of daily cycles is 0.3 m. Penetration of solar radiation into the snow can also be properly included in high-resolution time-dependent models.

In this study, the annual cycle of the thickness of landfast ice in the New Siberian Islands is examined using both an

analytical model[1] and a time-dependent thermodynamic model[18]. The models were forced by the surface heat fluxes, which were derived from observations at the Russian weather station Kotel'ny Island. The objectives were to investigate the annual variation of landfast ice thickness, in particular the maximum ice thickness and breakup date, for the site, and to examine the sensitivity of the annual sea ice thickness cycle to external forcing and parameterizations. Also the question of the absence of multi-year landfast ice was examined. The summer season, a critical part of the annual cycle, was examined through model simulations with known initial and final conditions.

2 Data and model

2.1 Ice season 2012–2013

The ice season August 2012–July 2013 was selected for the modelling investigations. MODIS and Landsat-8 satellite images were used to map the ice conditions in the season and to serve as the regional reference. The formation, stability and breakage of the landfast ice follow the evolution of ice thickness and strength[3,24].

High-resolution visible satellite images reflect well the real ice conditions and provided a direct insight into the ice seasons. The resolution of Landsat images is 30 m, which gives detailed information of the sea ice conditions. Additionally, MODIS images were used as a complement to monitor daily changes of the landfast ice zone. Based on their relatively coarse resolution (250 m), we obtained a good general picture about the evolution of the ice conditions.

The satellite data revealed that the landfast ice around Kotel'ny Island is seasonal. According to MODIS images, landfast ice on Siberian Shelf started to form in late October 2012 and soon filled the whole area. In 2013 mid-July, the landfast ice zone broke up and split into ice floes (Figure 2). The area was totally ice-free in mid-August, due to the melting, mechanical breakage and wind drift. Our modelled freezing and break-up dates (c.f. Section 3) are in line with these remote sensing observations. The Landsat-8 satellite images suggest that mechanical ice breakup took place prior to the total melting of the sea ice. Thus forcing by winds and tides played an important role in the ice breakup. E.g., in Prydz Bay, Antarctica, this often occurs in summer when the thickness of ice is less than about 50 cm[25-26].

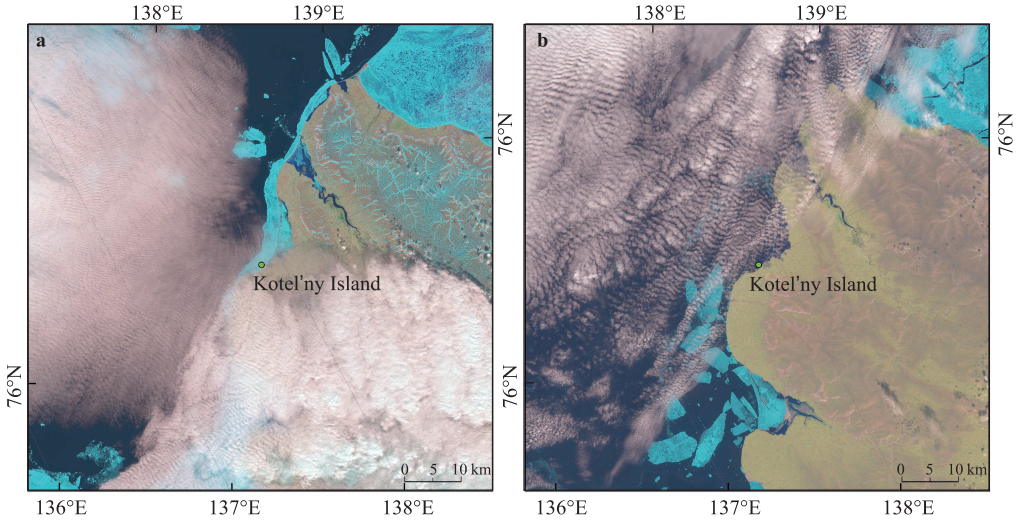

Figure 2 Landsat-8 images of coastal landfast sea ice west of Kotel'ny island. **a**, Image acquired on 2 July 2013; **b**, Image acquired on 17 July 2013. Blue areas represent ice.

Weather data were available from the Russian weather station Kotel'ny Island (76°00'N 137°52'E, altitude 8 m above sea level) located in the New Siberian Islands. Observations of wind speed and direction, air temperature, relative humidity, as well as cloudiness were available at 3-hour interval. Solar radiation was estimated using astronomical formulae for solar elevation and atmospheric corrections based in cloudiness and humidity[26-27]. *In situ* precipitation was not available; it is an external forcing factor for the modelling of snow thickness on sea ice. Historical investigations have indicated that the snow depth on landfast ice in southeastern Laptev Sea is 0.08 ± 0.05 m in April[28]. In Arctic coast, snowdrift is strong due to high wind speed[29]. This often results in less net snow accumulation. In this study, we used European Centre for Medium-Range Weather Forecasts (ECMWF) reanalyses of precipitation as the forcing; the horizontal resolution is about 80 km. The data were linearly interpolated into 1-hour interval for our modelling study. The time series of weather forcing are given in Figure 3.

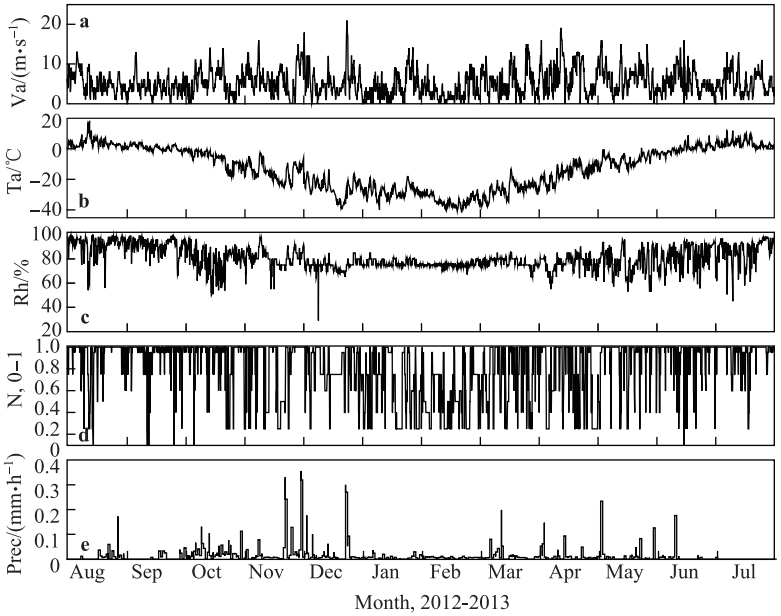

Figure 3 The time series of observed weather station data from 1 August 2012 to 31 July 2013. **a**, wind speed; **b**, air temperature; **c**, relative humidity; **d**, the cloudiness at Kotel'ny Island, and **e**, precipitation from ECMWF reanalyses.

The wind was strong (5.7 m·s^{-1}) in early winter months (Oct–Dec). Weak winds were observed in February (3.1 m·s^{-1}), while the maximum wind speed was measured in April (6.9 m·s^{-1}). The annual average wind speed was 5.3 m·s^{-1}, and the average wind speed was in winter months (Oct–May) 5.4 m·s^{-1}. The annual mean air temperature was −12.5°C, about 2°C warmer than the climatological mean value of −14.6°C (1935–2013). The winter mean air temperature was −20°C, while the average climatological mean air temperature in the cold season (Nov–Apr) is −24.4°C. The daily mean observed temperature and ECMWF reanalyses are compared in Figure 4. The correlation coefficient and RMSE between observed and ECMWF daily mean temperature were 0.96 and 3.3°C, respectively. In winter, the ECMWF temperature is overestimated, especially in February.

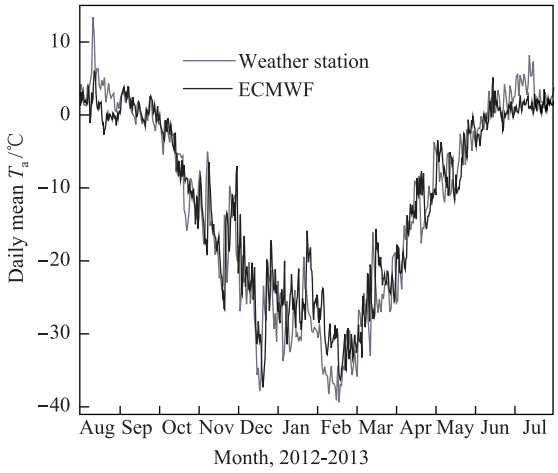

Figure 4 The time series of the daily mean air temperature at Kotel'ny Island Station and 12-hour mean air temperature from ECMWF reanalyses.

2.2 Thermodynamic modelling of sea ice

Most of Arctic sea ice is congelation ice. Ice crystals grow from the ice bottom, and the released latent heat is conducted through the ice to the atmosphere. Heat transfer is in the vertical direction, since the lateral length scales are much larger than vertical. The basic equation is therefore the vertical heat conduction law[1, 4, 20]:

$$\rho c \frac{\partial T}{\partial t} = \frac{\partial}{\partial z}\left(k \frac{\partial T}{\partial t} - Q_{s+}\right) \tag{1}$$

Where ρ is ice density, c is specific heat of ice, k is thermal conductivity, T is temperature, t is time, z is vertical coordinate positive downward, and Q_{s+} is the solar radiation in the ice. For sea ice, the heat capacity ρc and the thermal conductivity depend on the temperature and salinity, while for snow they depend on the density. The bottom boundary condition provides the growth of congelation ice:

$$z = h_d : T = T_f,\ \rho L \frac{\mathrm{d}h}{\mathrm{d}t} + Q_w = k \frac{\partial T}{\partial z} \tag{2a}$$

where T_f is the freezing point temperature, h is ice thickness, h_d is draft, L is the latent heat of freezing, and Q_w is the oceanic heat flux. The surface boundary condition is:

$$z = h_f : \rho L \frac{\mathrm{d}h}{\mathrm{d}t} + Q_0 = k \frac{\partial T}{\partial z};\ \frac{\mathrm{d}h'}{\mathrm{d}t} = \frac{\rho_w}{\rho}(P - E) + \frac{\rho_s}{\rho} D \tag{2b}$$

Where h_f is freeboard, Q_0 is the surface heat balance, ρ_w is water density, h' is atmospheric surface mass flux, P and E are precipitation and sublimation, respectively, and D is net snow drift. Eqs. (2a, 2b) give the bottom and surface heat and mass balances.

The surface heat balance is written in detail as

$$Q_0 = (1-\alpha)(1-\gamma)Q_s + \varepsilon\sigma(\varepsilon_a T_a^4 - T_0^4) + Q_e + Q_c + Q_p \tag{3}$$

where Q_s is the incoming solar radiation, α is albedo, γ is the fraction of the net solar radiation penetrating the surface, ε

is the thermal emissivity of the surface, ε_a=(0.746+0.066 mbar$^{-1/2}$ $\sqrt{e}$)×(1+0.26N) is the effective thermal emissivity of atmosphere, e is water vapour pressure, N is cloudiness ($0 \leqslant N \leqslant 1$), σ is Stefan-Boltzmann constant, T_a and T_0 are the air and surface temperature, respectively, Q_e and Q_c are the latent and sensible heat fluxes, respectively, and Q_P is the heat flux from precipitation. The last term is significant only when there are phase changes involved.

Frazil ice, snow-ice and platelet ice are not considered here, since their contribution to the ice growth is assumed small in the study region. In general, frazil ice may form when there is open water present but here that has likely not much influence to the maximum annual ice thickness. The heat loss for the frazil ice formation is obtained from Eq. (3) taking the surface temperature equal to the freezing point. Snow-ice does not form since the snow cover is thin and dry. Platelet ice growth is an important mechanism in parts of the Antarctic landfast ice[30]; in principle it can be found in Arctic river mouths as, e.g., in Saroma-lagoon of the Sea of Okhotsk[31]. This has, however, not been reported in landfast sea ice studies in the Laptev Sea ice[32], and for East Siberian Sea no work is known to the present authors. It still remains unknown to what degree frazil ice formation takes place and whether platelet ice forms in Siberian river mouths.

In this work the time-dependent model HIGHTSI[18,21,26-27] is employed for the congelation ice. The model solves the heat conduction equation (1) with the boundary conditions (Eqs. 2–3) in the snow and ice layers for the evolution of temperature and thickness of ice and snow. At the upper boundary, the solar and terrestrial radiative fluxes and the turbulent heat fluxes are parameterized, with the turbulent fluxes taking into account the stability of atmospheric stratification[21]. The surface temperature is solved from the surface energy balance that couples the snow and ice sheet with the atmosphere. Oceanic heat flux is prescribed as a function of time, Q_w=$Q_w(t)$, not coupled to the ice model, since a proper treatment of the boundary layer beneath the ice is missing from the model.

The thickness and density of new snow are taken from precipitation assuming a given density. In the course of time, snow density is changed due to packing determined by wind and temperature. The thermal conductivity of snow is parameterized based on its density[33]. Both albedo and light attenuation coefficient are important for the solar radiation transfer. Albedo depends on the surface conditions (snow/ice and dry/wet), and its time evolution is a major question in the melting season due to the presence of liquid water.

An attenuation law similar to Bouguer-Lambert absorption law is employed for the radiation transfer inside the snow and ice with κ as the attenuation coefficient. Ice and snow have their own attenuation coefficients, and, additionally, the topmost 10-cm layer has a larger attenuation coefficient. This treatment of the top layer reflects the rapid attenuation of ultraviolet and near-infrared wavelengths close to the surface. The fraction i_0, radiation absorbed in the top layer, depends on the cloudiness N and the ice type; for clear congelation ice, $i_0 = 0.43\times(1-N) + 0.63\times N$[34-35]. A more sophisticated method to calculate the solar radiation transfer in snow and ice would be an advanced transfer scheme[36]. A comparison has shown, however, that the results based on the linear attenuation law are close to Liston's[36] advanced scheme, in particular for the snow layer[37].

The vertical grid contains 10 grid cells in snow and 20 grid cells in ice, and at the maximum ice thickness of 2 m the physical grid step is 10 cm. The grid size is small enough to resolve the daily cycles in ice temperature and thickness. The model parameters are given in Table 1.

Table 1 The model parameters applied for this study

Parameter	Value	Source
Albedo/α	Function of h_i, h_s	Reference [35]
Attenuation coefficient	Function of h_i, N	
- of sea ice/κ_i	1.5 – 17 m^{-1}	Reference [34]
- of snow/κ_s	15 – 25 m^{-1}	Reference [35]
Freezing point of sea water/T_f	–1.8℃	Sea water (35‰ salinity)
Initial density of snow/ρ_{so}	320 kg·m^{-3}	Reference [38]
Sea ice volumetric heat capacity/ρc_i	Function of T_i, s_i	Reference [39]
Sea ice density/ρ	910 kg·m^{-3}	Representative at the site
Sea ice salinity/s_i	4‰	Representative at the site
Snow density/ρ_s	Time dependent	Reference [40]
Surface emissivity/ε	0.97	General reference
Thermal conductivity of sea-ice/k_{si}	Function of T_i, s_i	Reference [39]
Thermal conductivity of snow/k_s	Function of ρ_s	Reference [33]
Time step of model/t	3 600 s	Model configuration
Number of layers in the ice	20	Model configuration
Number of layers in the snow	10	Model configuration

Note: h_i, h_s are snow and ice thicknesses, N is cloudiness, and T_i is ice temperature.

3 Results

3.1 Scaling of the annual cycle

We can obtain the scaling of the ice thickness cycle by analytic quasi-steady models[1]. The basic model is[1,3]:

$$\rho L \frac{\mathrm{d}h}{\mathrm{d}t} + Q_w = k \cdot \frac{T_f - T_0}{h} = Q_0(T_0, T_a) \quad (4)$$

This formula gives a good approximation for the growth of ice, based on the heat transfer through the ice and atmospheric surface layer, and analytic solution can be obtained when the oceanic heat flux is ignored. The rate of melting can be taken as a function of the heat fluxes at the top and bottom surfaces. Then the solutions for the annual growth (assuming $Q_w = 0$) and melting of sea ice become:

$$h_1 = \sqrt{aS + d^2} - d,\ a = \frac{2k}{\rho L} \quad (5a)$$

$$\Delta h = \frac{<Q_0 + (1-a)Q_s> + <Q_w>}{\rho L} \tau_m \quad (5b)$$

where h_1 is the first-year-ice thickness, S is the sum of freezing-degree-days (below the freezing point), d describes atmospheric surface layer buffering of heat transfer from the ice sheet, Δh is summer melt, τ_m is the length of summer, and the notation <·> stands for time averaging. Eq. (5a) is the Zubov solution[3], while Eq. (5b) comes from the heat balance integral over the melting period[26]. The length of the summer can be taken as the period when the sum of the total surface heat flux $Q_0 + (1-a)Q_s$ stays positive. In the study year, the mean air temperature was –20°C during the ice growth season (Oct–May), in Jan–Feb the minimum was –41°C, and the freezing-degree-days summed to S =4 781°C·d.

The original Zubov's[3] parameters were a = 8 cm^2·°C^{-1}·d^{-1} and d = 25 cm, while later[1] a theoretical value of a = 11 cm^2·°C^{-1}·d^{-1} and en empirical value d = 10 cm have been used as representative values. The latter parameterization worked well in almost snow-free site in Prydz Bay, East Antarctica[26], while Zubov's[3] semi-empirical parameterization maybe better representative of the particular conditions on the Siberian coast. The resulting maximum annual thickness of first-year sea ice, using 2012-2013 Kotel'ny Island weather station data, was 172 cm with the Zubov's parameters[3].

The air temperature was above 0°C from April. To estimate the melt rate of ice, the positive degree-day method has been widely used in sub-polar regions with a melt rate of 0.5 cm·°C^{-1}·d^{-1} while in high Arctic values of 1 cm·°C^{-1}·d^{-1} have been obtained in Canadian lakes[41]. By the end of August, positive air temperatures summed to 226°C·d, which means that the amount of ice melt would be 113–226 cm. However, the break-up date was rather close to the end of July, and therefore the analytic analysis suggests that melting together with ice breakage and drift were the cause of disappearance of the landfast ice in summer, preventing the formation of multiyear ice.

3.2 HIGHTSI experiment

The external forcing for HIGHTSI is based on the air temperature, wind speed, relative humidity, cloudiness, precipitation, and incoming solar and atmospheric radiation. Snow cover is modelled from precipitation and metamorphic processes. The initial ice thickness was taken as 2 cm. To obtain the annual ice thickness cycle, the basic simulation started with the freezing date of 8 October and was run until 31 August of the following year. These simulations showed how the ice could decay and how the next ice season was to begin. The site opened by mid-July–mid-August, due to melting and mechanics (breakage and drift), depending on the model parameterization. We carried out a number of model sensitivity experiments, and in each experiment, one external factor was changed for each experiment (Table 2), and the standard experiment was fixed by Exp D+I+P. In the resulting figures below the vertical zero level always refers to the top surface of the ice. Therefore only total change in ice thickness, top and bottom melting together, is seen.

Table 2 Model experiments with various combinations of external forcing

Factor	Parameterization	Model experiment
Albedo	0.5	Exp A
	0.6	Exp B
	0.7	
	0.8 for dry snow 0.7 for melting snow	Exp C
	0.5 for dry ice 0.3 for melting ice	Exp D
Oceanic heat flux	0 W·m^{-2}	Exp E
	5 W·m^{-2}	Exp F
	15 W·m^{-2}	Exp G
	25 W·m^{-2}	Exp H
	October—May, 2 W·m^{-2} June—July, 2 –>25 W·m^{-2}	Exp I
Air temperature	Observation +1°C	Exp J
	Observation −1°C	Exp K
	Observation +2°C	Exp L
	Observation −2°C	Exp M
Precipitation	0	Exp N
	ECMWF	Exp P
	2×ECMWF	Exp Q

The summer period is the most uncertain time because of rapid rate of melting and the sensitivity to forcing and parameterization. The factors selected for these sensitivity experiments were albedo, oceanic heat flux, snow accumulation and air temperature, which produce the main uncertainties in the summer simulations. Melting of ice is mainly due to solar radiation and oceanic heat flux. Air temperature sensitivity is largely related to turbulent heat fluxes, which may be important especially in the coastal zone, and the role of snow is to strongly influence the start-up of ice melting. Note that melting of ice is nearly additive, i.e. independent of the melting in the previous day or week, so that total melting is provided by total heat gain during the period of concern.

Figure 5 shows the time series of the modelled ice thickness cycle for the different parameterizations of albedo. The ice thickness is not much affected by the albedo in the growth season, only from spring when the solar radiation reaches a significant level. Large differences are seen in summer. With $\alpha = 0.5$ ice melts completely by the middle of July while with $\alpha = 0.7$ the ice has disappeared in the middle of August, which reflect too much and too little melting, respectively. With $\alpha = 0.6$, the breakup of ice is at 28 July. For small changes of albedo, the sensitivity of the break-up date t_b is $\delta t_b \sim -\delta\alpha \times 150$ d.

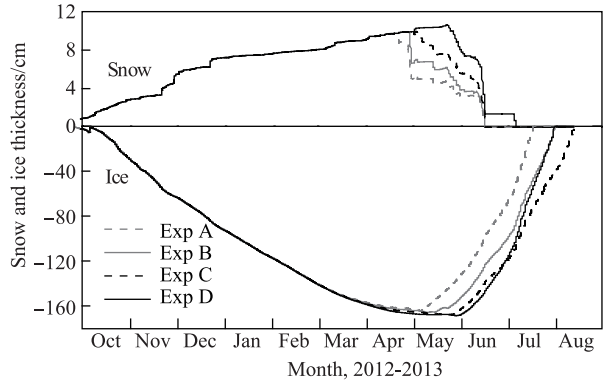

Figure 5 The modelled annual snow and ice thickness in terms of different surface albedo conditions. The oceanic heat flux was 2 W·m^{-2} in winter and increased to 25 W·m^{-2} in summer (Exp I). Note the different scale of snow and ice thickness (also in Figures 6, 7, 8 and 9). The zero level refers to the top surface of the ice.

The oceanic heat flux was assumed to be within a range from 2 up to 25 W·m^{-2}. Figure 6 shows the sensitivity result for the summer oceanic heat flux. Here the albedo was within 0.3–0.8 depending on the state of the surface (Exp D). The modelled ice breakup ranged within half a month. With a fixed 15 W·m^{-2} oceanic heat flux, melting rate of ice was 3.2 cm·d^{-1}. It is clear from the simulations that the oceanic heat flux must increase during summer so that in July the level is again at 25 W·m^{-2}. We obtained from the simulations

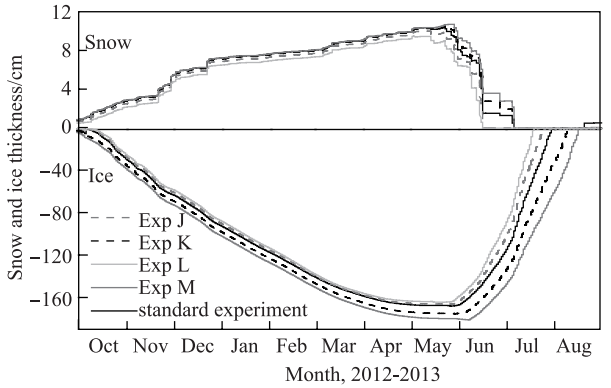

Figure 6 The modelled annual snow and ice thickness in terms of different oceanic heat flux conditions. The surface albedo was from 0.3 (wet ice) to 0.8 (dry snow) according to Exp D. The zero level refers to the top surface of the ice.

that the sensitivity of the breakup date to the oceanic heat flux is $\delta t_b \sim -\delta Q_w$(W·m^{-2})$^{-1} \times 1$ d.

By the success of freezing-degree-day models, it is clear that the ice growth is largely determined by the air temperature. In the case ice reaches thicknesses more than 1 m, the sensitivity of the ice thickness to air temperature is not high (Figure 7), from the analytic model we have $\delta h \sim \frac{1}{2} a \times h^{-1} \times \delta S$. However, in the melting season the turbulent heat fluxes are important, and with temperature ±2°C from the mean, the range in the ice break-up date becomes 30 d, i.e. $\delta t_b \sim -\delta T$°C$^{-1} \times 15$ d.

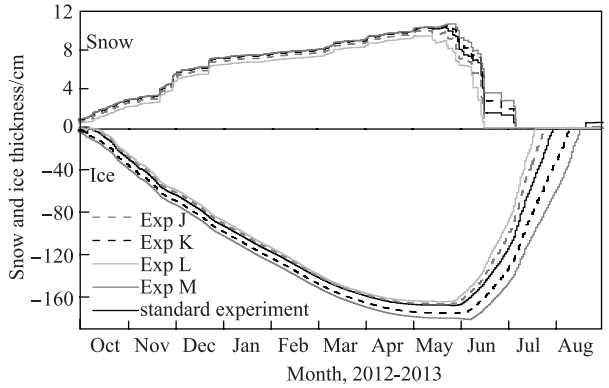

Figure 7 The sensitivity of annual snow and ice thickness cycle to the changes of air temperature. The observed time series and that ±1°C and ±2°C are used. The zero level refers to the top surface of the ice.

In the Arctic seas, snow adds on the insulation in the growth season and protects the ice from melting in summer. In our case, no snow and doubled snow thickness gave the thicknesses from 120 cm to 219 cm, respectively, while the standard case gave 167 cm (Figure 8). Also the more there was snow, the later the melting of ice started, and the range in the ice breakup date was 35 d.

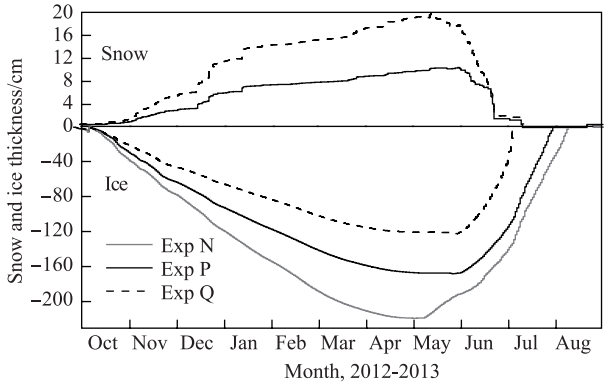

Figure 8 The simulated snow and ice thickness using different precipitation patterns: Exp P – observed, Exp N – none, and Exp Q – double. The zero level refers to the top surface of the ice.

4 Discussion

The annual cycle of snow and ice temperature and thickness reflects the cold growth season of Oct–May and the short

summer (Jun–Aug). In the study year, the ice thickness grew steadily, and the temperature in the ice surface layer was below –30°C at coldest and at 1 m depth the temperature was higher than –15°C (Figure 9). In summer the ice was isothermal.

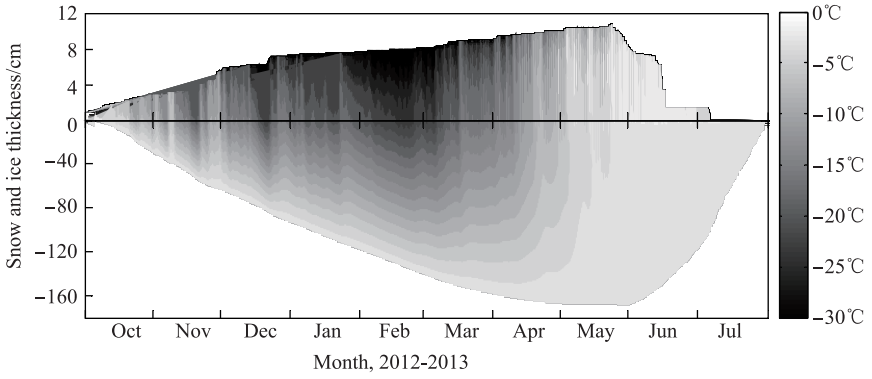

Figure 9 Snow and ice temperature and thickness in October 2012–July 2013 as produced by HIGHTSI standard experiment.

The heat budget is shown in Figure 10. The surface of the ice varied between bare state and thin snow cover, and all summer the surface was bare. The longwave radiation makes an annual cycle dictated by the temperature and cloudiness, while net solar radiation is weak in winter, jumping fast to high levels in the melting season when the albedo decreases. For a latent heat flux of –30 W·m^{-2}, mass loss by sublimation would be 1 mm·d^{-1}. In the growth season, because of the cold conditions, the latent heat flux is about –20 W·m^{-2}, but in summer the ice thickness would decrease by about 4 cm due to sublimation.

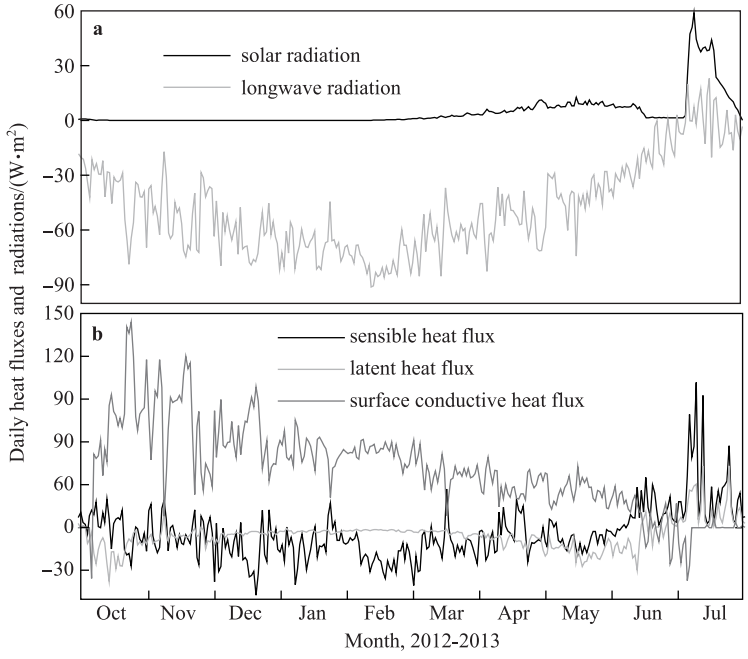

Figure 10 The HIGHTSI modelled surface heat fluxes (daily mean) for standard experiment.

The surface heat fluxes reflect the ice growth and melt. Components of monthly surface energy balance were calculated for the standard experiment (Table 3). The net longwave radiation dominates the surface heat balance in the winter season, while the net solar radiation is critical for melting. The weather conditions in early winter and in early spring are critical for the determination of the length of the ice season. The positive surface heat balance led to the rapid melting and breakup of landfast ice in July.

Finally, the potential multi-year ice cycle of ice thickness was simulated by HIGHTSI. This was done without including any mechanical ice losses. The standard parameters were used: albedo equal to 0.6, and the oceanic heat flux linearly decreasing from 25 W·m^{-2} to 2 W·m^{-2} from October to May, and then in June–July it was linearly increased back to 25 W·m^{-2}. The resulting simulation approached asymptotically 161 cm at maximum, which is 11 cm lower than obtained by the analytical model (Eq. 6). The reason is

that the analytic model did not account for the oceanic heat flux in the ice growth season. The resulting summer melt was equal to the growth, leaving an open water period of about 1.5 months. This is quite long and means that ice may disappear by melting but mechanical breakage and drift of ice, if occurs, produces an earlier breakup date than pure thermodynamics. Taking the melt rate of 3 cm·d^{-1} and the ice thickness at breakage[3,26], this means that the open water period may be 15–30 d longer due to mechanics. The oceanic heat flux is one more important parameter to control the ice melting in summer.

Table 3 The monthly mean heat fluxes contributing to the surface heat balance (W·m^{-2}) in October 2012—July 2013. The columns are surface layer absorption of solar radiation (Q_s), net longwave radiation (Q_l), latent heat flux (Q_e), sensible heat flux (Q_c), conductive heat flux from below (F_c), all fluxes are positive towards the surface. Total solar radiation absorption and total monthly fluxes are 44.75 W·m^{-2} and −123.45 W·m^{-2}, respectively. Fluxes are taken positive when directed toward ice.

	Oct.	Nov.	Dec.	Jan.	Feb.	Mar.	Apr.	May	Jun.	Jul.
Q_s	0.18	0.00	0.00	0.00	0.25	2.00	5.77	8.77	4.55	23.23
Q_l	−38.14	−49.76	−63.81	−68.64	−78.08	−63.95	−55.29	−41.70	−22.33	−0.59
Q_e	−13.40	−5.80	−4.68	−2.79	−1.97	−3.52	−8.47	−16.51	−6.16	12.43
Q_c	−0.35	−3.25	−16.18	−11.01	−20.10	−13.44	−4.45	−7.93	9.57	26.80
F_c	64.48	72.05	63.96	53.00	52.79	39.06	30.02	25.60	7.74	−3.40

Unfortunately, we do not have any *in situ* snow and ice thickness observations from study site. A landfast sea ice survey in the previous ice season (2011) in Sogo Bay in Tiksi Gulf (Figure 1) revealed that the maximum thickness of landfast ice exceeded 2 m[42]. Tiksi is located south of Kotel'ny Island, and the thicker landfast ice maybe resulted by the cold continental climate dominated by the Siberian high pressure. The annual climatological mean air temperatures in Tiksi and Kotel'ny Island were –13°C and –15°C, respectively, and during early ice season (Oct— Feb), the climatological mean air temperatures in Tiksi and Kotel'ny Island were –25°C and –24°C, respectively. The colder temperature in the ice season in Tiksi results thicker landfast sea ice compared with that in Kotel'ny Island, 2°C can produce 15% more ice thickness[3]. In addition, the landfast ice around Tiksi is affected by fresh water inflow from rivers. Previous studies indicated that the fresh water ice can be at least 10% thicker than the sea ice formed by saline water[43].

In Kotel'ny Island, the wind was strong. The monthly average wind speed in winter (Oct— May) was 5.4 m·s^{-1}. A strong wind may contribute to spatial inhomogeneity of snow distribution in early winter season, which eventually affects the regional heat conductivity of snow[18]. A sensitivity experiment suggested that increase of snow heat conductivity from 0.3 to 0.5 W·m^{-1}·°C $^{-1}$ in early ice season would result in 20 cm more maximum ice thickness and a week delay of ice breakup date.

5 Conclusions

The annual cycle (2012—2013) of landfast sea ice thickness west of Kotel'ny Island between Laptev Sea and East Siberian Sea was investigated in this study. The remote sensing data was used for landfast ice detection. The *in situ* weather station data was used as the driving force for the annual cycle of landfast ice. A one-dimensional, time-dependent thermodynamic snow and ice model (HIGHTSI) was applied to simulate the annual variation of sea ice thickness. A number of model experiments were carried out to study the sensitivity of various external factors on variation of snow and ice thickness.

Under clear sky condition, high-resolution Landsat images are very useful to understand the detail mechanical features of landfast ice, in particular ice breakup. MODIS images are also applicable to be used for landfast ice monitoring. The annual temperature of 2012–2013 was warmer than average climatological condition in New Siberian Islands. The daily mean air temperature dropped below 0°C on 26 September. Compared with average climatological condition, the summer (August) was warmer.

The freezing-degree-days were 4 781°C·d in the ice growth season in 2012–2013. This was 990°C·d smaller than the average seasonal freezing-degree-days. The annual maximum modelled ice thickness of 2012–2013 season was 172 cm. Scaling analysis by analytical models was also elaborated for the multi-year ice equilibrium cycle and the annual maximum ice thickness. The time dependent sea ice thermodynamic model HIGHTSI was also used to examine the annual cycles of ice thickness and temperature and their sensitivity to the forcing. The standard reference model run yields 167 cm seasonal maximum ice thickness. Both values are smaller than the maximum landfast ice thickness measured in Sogo Bay around Tiksi[42]. Tiksi is located south of Kotel'ny Island, but the mean daily air temperature was there a little colder than that in Kotel'ny Island in Oct—Nov and Jan—Feb; Kotel'ny Island is more dominated by the marine environment and the weather was not that cold as in Tiksi. The landfast ice around Tiksi was also affected by the fresh water inflow from rivers. Some early studies indicated that the fresh water ice could be at least 10% thicker than the ice formed by saline water ice[43].

Without snow, the ice thickness can reach 220 cm in

Kotel'ny Island. The effect of precipitation on ice thickness is very complicated owning to the fact that precipitation is highly dynamic, especially in early winter season[44]. In the Arctic Ocean, the portions of precipitation contributing to the snow accumulation or snowdrift are highly dependent on the synoptic weather condition and the cyclone activities. In an Arctic lake, snowfall in early winter season can contribute significantly to the total ice thickness by forming of snow-ice[45], but in the Eurasian Arctic coast the challenges remain not only to assess the correct quantity of precipitation but also the observed snow thickness. The effects of wind can make *in situ* precipitation measurements liable to as large as 200% errors[46]. To tackle these challenges further field measurements and modelling studies are needed.

Sensitivity studies were particularly made for the summer season to close the ice thickness cycle. The melting and breakup of ice is the most difficult part of the ice season to model. Sensitivity analyses were made for the albedo, oceanic heat flux, air temperature, and snow accumulation. They were all important factors, and realistic ranges of variability produced about one month range in the date of ice breakup. In summer, sublimation can add 4 cm to the loss of ice, based on the modelled latent heat. Melt ponds were not explicitly treated but they are reflected in the albedo algorithm.

The continuation of this research needs more work on the ice break-up process using high-resolution satellite data. The question about ice disappearance needs the understanding of the mechanical breakage of ice, which is a challenging task due to the highly variable strength of the warm summer ice. In two-dimensional ice-ocean models, landfast ice zone is not well represented for its physics but it has an important role in the decay process when it breaks and drifts away.

The Arctic is expected to have ice-free summers within the next few decades[47]. Better understanding of the sea ice thickness near the coastal region is important. The results guide understanding of the sea ice thickness in the Eurasian coast.

Acknowledgments The ECMWF is acknowledged for data supply. The authors are supported by research funding from the National Natural Science Foundation of China (Grant nos. 41428603, 41376186, 41476170); the EU FP7 Project EuRu CAS(European-Russian Centre for Cooperation in the Arctic and Sub-Arctic Environmental and Climate Research, Grant no. 295068); Academy of Finland (Grant nos. 11409391, 259537); the Liaoning Educational Committee Foundation (Grant no. L2013497), and the Ocean Public Welfare Scientific Research Project of China (Grant nos. 201205007, 201205007-2).

References

1 Leppäranta M. A review of analytical models of sea-ice growth. Atmos Ocean, 1993, 31(1): 123–138
2 Weeks W F, Ackley S F. The growth, structure, and properties of sea ice // Untersteiner N. The geophysics of sea ice. New York: Plenum Press, 1986
3 Zubov N N. L'dy Arktiki Moscow: Izdatelstvo Glavsevmorputi, English translation (Arctic ice)1963, Washington DC: Naval Oceanographic Office, 1945 (in Russian)
4 Maykut G A, Untersteiner N. Some results from a time-dependent thermodynamic model of sea ice. J Geophys Res, 1971, 76(6): 1550–1575
5 Kwok R, Cunningham G F, Wensnahan M, et al. Thinning and volume loss of the Arctic Ocean sea ice cover: 2003–2008. J Geophys Res, 2009, 114(C7): C07005, doi:10.1029/2009JC005312
6 Rodrigues J. The rapid decline of the sea ice in the Russian Arctic. Cold Reg Sci Technol, 2008, 54(2): 124–142
7 Eicken H, Lensu M, Leppäranta M, et al. Thickness, structure, and properties of level summer multiyear ice in the Eurasian sector of the Arctic Ocean. J Geophys Res, 1995, 100(C11): 22697–22710
8 Walker E R, Wadhams P. Thick sea-ice floes. Arctic, 1979, 32(2): 140–147
9 Reimnitz E, Eicken H, Martin T. Multiyear fast ice along the Taymyr Peninsula, Siberia. Arctic, 1995, 48(4): 359–367
10 Polyakov I V, Alekseev G V, Bekryaev R V, et al. Long-term ice variability in Arctic marginal seas. J Climate, 2003, 16(12): 2078–2085
11 Dmitrenko I A, Kirillov S A, Tremblay L B. The long-term and interannual variability of summer fresh water storage over the eastern Siberian shelf: Implication for climatic change. J Geophys Res, 2008, 113(C3): C03007, doi:10.1029/2007JC004304
12 Sirevaag A, Fer I. Early spring oceanic heat fluxes and mixing observed from drift stations north of Svalbard. J Phys Oceanogr, 2009, 39(12): 3049–3069
13 Fer I, Skogseth R, Geyer F. Internal waves and mixing in the Marginal Ice Zone near the Yermak Plateau. J Phys Oceanogr, 2010, 40(7): 1613–1630
14 Shoutilin S V, Makshtas A P, Ikeda M, et al. Dynamic-thermodynamic sea ice model: ridging and its application to climate study and navigation. J Climate, 2005, 18(18): 3840–3855
15 Leppäranta M. A growth model for black ice, snow ice and snow thickness in subarctic basins. Nordic Hydrol, 1983, 14(2): 59–70
16 Semtner A J. A model for the thermodynamic growth of sea ice in numerical investigations of climate. J Phys Oceanogr, 1976, 6(3): 379–389
17 Winton M. A reformulated three-layer sea ice model. J Atmos Ocean Technol, 2000, 17: 525–531
18 Launiainen J, Cheng B. Modelling of ice thermodynamics in natural water bodies. Cold Reg Sci Technol, 1998, 27(3): 153–178
19 Bitz C M, Lipscomb W H. An energy-conserving thermodynamic model of sea ice. J Geophys Res, 1999, 104(C7): 15669–15677, doi:10.1029/1999JC900100
20 Saloranta T M. Modeling the evolution of snow, snow ice and ice in the Baltic Sea. Tellus, 2000, 52(1): 93–108
21 Cheng B, Launiainen J, Vihma T. Modelling of superimposed ice formation and sub-surface melting in the Baltic Sea. Geophysica, 2003, 39(1–2): 31–50
22 Shirasawa K, Leppäranta M, Saloranta T, et al. The thickness of coastal fast ice in the Sea of Okhotsk. Cold Reg Sci Technol, 2005, 42(1): 25–40
23 Vancoppenolle M, Fichefet T, Goosse H, et al. Simulating the mass balance and salinity of Arctic and Antarctic sea ice. 1. Model description and validation. Ocean Modelling, 2009, 27(1–2): 33–53, doi:10.1016/j.ocemod.2008.10.005
24 Leppäranta M. The Drift of Sea Ice, 2nd edition. Heidelberg, Germany: Springer-Praxis, 2011: 347
25 Lei R B, Li Z J, Cheng B, et al. Annual cycle of landfast sea ice in Prydz Bay, east Antarctica. J. Geophys Res, 2010, 115(C2): C02006,

doi:10.1029/2008JC005223
26 Yang Y, Li Z, Leppäranta M, et al. Modeling the thickness of landfast sea ice in Prydz Bay, East Antarctica with a focus on summer decay. Antarctic Science, 2015, accepted for publication
27 Cheng B, Zhang Z H, Vihma T, et al. Model experiments on snow and ice thermodynamics in the Arctic Ocean with CHINARE 2003 data. J Geophys Res, 2008, 113(C9): C09020, doi:10.1029/2007JC004654
28 Gudkovich Z M, Gladkov M G, Luk'ianchikov S N. Ice cover volume and ice thickness distribution on the southeastern part of the Laptev Sea at the end of the winter 1976 (in Russian) // Treshnikov A F. Polex-North-76 (Scientific Results) Part 2. Gidrometeoizdat, Leningrad, 1979: 16–19
29 Jaedicke C, Thiis T, Sandvik A D, et al. Drifting snow in complex terrain-comparison of measured snow distribution and simulated wind field. Proceedings of the Fourth International Conference on Snow Engineering. Trondheim, Norway, 2000: 65–73
30 Smith I J, Langhorne P J, Haskell T G, et al. Platelet ice and the land-fast sea ice of McMurdo Sound, Antarctica. Ann Glaciol, 2001, 33(1): 21–27
31 Shirasawa K, Leppäranta M. Measurements and modeling of the ice–ocean heat flux // Eicken H, Gradinger R, Salganek M, et al. Field techniques in sea ice research. Fairbanks, AK: University of Alaska Press, 2009
32 Eicken H, Reimnitz E, Alexandrov V, et al. Sea-ice processes in the Laptev Sea and their importance for sediment export. Cont Shelf Res, 1997, 17(2): 205–233
33 Sturm M, Holmgren J, König M, et al. The thermal conductivity of seasonal snow. J Glaciol, 1997, 43(143): 26–41
34 Grenfell T C, Maykut G A. The optical properties of ice and snow in the Arctic Basin. J Glaciol, 1977, 18: 445–463
35 Perovich D K. The Optical Properties of Sea Ice. CRREL Report 96–1. Hanover NH: Cold Regions Research and Engineering Laboratory, 1996
36 Liston G E, Winter J G, Bruland O, et al. Below-surface ice melt on the coastal Antarctic ice sheet. J Glaciol, 1999, 45(150): 273–285
37 Cheng B. On the numerical resolution in a thermodynamic sea-ice model. J Glaciol, 2002, 48(161): 301–311
38 Semmler T, Cheng B, Yang Y, et al. Snow and ice on Bear Lake (Alaska)–sensitivity experiments with two lake ice models. Tellus A, 2012, 64: 17339. doi:10.3402/tellusa.v64i0.17339
39 Pringle D J, Eicken H, Trodahl H J, et al. Thermal conductivity of landfast Antarctic and Arctic sea ice. J Geophys Res, 2007, 112(C4): C04017, doi:10.1029/2006JC003641
40 Anderson E A. A point energy and mass balance model of a snow cover. Tech. Rep. NWS 19, Natl. Oceanic and Atmos. Admin., Washington, D. C., 1976
41 Mueller D R, Van Hove P, Antoniades D, et al. High Arctic lakes as sentinel ecosystems: Cascading regime shifts in climate, ice cover, and mixing. Limnol Oceanogr, 2009, 54(6, part 2): 2371–2385
42 Makshtas A P, Bogorodskiy P V, Kustov V Y. Rapidmelt of landfast-ice in Sogo Bey (Tiksi Gulf) during spring 2011. Problems of Arctic and Antarctic, 2012, 1: 37–47 (in Russian)
43 Eicken H, Grenfell T C, Perovich D K, et al. Hydraulic controls of summer Arctic pack ice albedo. J Geophys Res, 2004, 109(C8): C08007, doi:10.1029/2003JC001989
44 Cheng B, Mäkynen M, Similä M, et al. Modelling snow and ice thickness in the coastal Kara Sea, Russian Arctic. Ann Glaciol, 2013, 54(62): 105–113
45 Cheng B, Vihma T, Rontu L, et al. Evolution of snow and ice temperature, thickness and energy balance in Lake Orajärvi, northern Finland. Tellus A, 2014, 66: 21564, http://dx.doi.org/10.3402/tellusa.v66.21564
46 Aleksandrov Y I, Bryazgin N N, Førland E J, et al. Seasonal, interannual and long-term variability of precipitation and snow depth in the region of the Barents and Kara seas. Polar Res, 2005, 24(1–2): 69–85, doi:10.1111/j.1751-8369.2005.tb00141.x
47 Wang M Y, Overland J E. A sea ice free summer Arctic within 30 years? Geophys Res Lett, 2009, 36: L07502. doi:10.1029/2009GL037820